Engineering Science and Technology, an International Journal xxx (xxxx) xxx

HOSTED BY

ELSEVIER

Contents lists available at ScienceDirect

Engineering Science and Technology, an International Journal

journal homepage: www.elsevier.com/locate/jestch

Full Length Article

Electrical and physical characterization of earth faults for diverse bush species

Cagil Ozansoy *, Douglas Pinto Sampaio Gomes

College of Engineering and Science, Victoria University, PO Box 14428, Melbourne, Vic 8001, Australia

ARTICLE INFO

Article history:
Received 2 September 2019
Revised 23 January 2020
Accepted 7 March 2020
Available online xxxx

Keywords:
Bush fires
Conduction continuity
High impedance fault
Ignition stages
RMS fault current

ABSTRACT

High Impedance Faults (HIFs) are disturbances with a potential to ignite bush fires. This work focuses on presenting physical and electrical phenomena associated with earth faults for a range of bush species. Phase to earth bush faults are analyzed in terms of the fault current limit and speed/nature of the fault current's development. HIFs that lead to fires are shown to differ in terms of conduction continuity from those that do not result in ignition. Three stages of ignition development are investigated governing the physical phenomena of ignition of a bush species under a HIF scenario. The change Δ in the averaged fault RMS current is shown to yield patterns that signify various stages of ignition. In particular, the first zero-crossing in the Δ has been shown to correlate to the point when ignition progresses from initial contact stage to the moisture expulsion stage.

1. Introduction

HIFs occur when a conductor comes into contact with a high impedance surface, resulting in small currents insufficient to operate conventional protection schemes. If undetected, HIFs pose a severe risk to public safety and can ignite fires. The HIF current is characterized by a low magnitude, unstable, and fluctuating current [1]. Typical features of HIFs reported in the literature are non-linearity, asymmetry, intermittency, and randomness [2]. HIF models are predominantly based on arc modelling as well as the non-linear resistance of the high impedance fault [2,3]. Despite widespread efforts on HIF modelling, the link between HIF current buildup and development of ignition in vegetation is poorly investigated.

Detection and localization of faults in distribution networks always been at the forefront of research [4–6]. Centralized methods based on artificial intelligence and travelling waves [7] as well as those requiring high-speed sampling [8] are becoming popular. Ghaderi et. al. define HIF detection as a process with steps of signal measurement, feature extraction, and classification to distinguish a faulty signal from a healthy one[9]. For example, superimposed components of the residual voltage at the substation bus was used by Sarwagya et. al. for discriminating HIFs from other power system disturbances [10]. Alternatively, Chaitanya et. al. used variational mode decomposition for feature extraction fed into a support vector machine classifier [11]. However, despite many methods proposed in the literature for HIF detection, few have put any emphasis on the electrical and physical characterization of earth faults. The present paper makes an attempt to address this problem.

Studies on the electrical and physical characterization of earth vegetation faults have been fewer; the key shortcoming addressed in this work. Comparable work on the characterization of the physical and electrical phenomena associated with vegetation contacts on distribution conductors was previously presented in [12]. The key conclusion was that initial current levels were low and the fault current peaked as carbonization increased. Whilst pioneering, the work in [12] did not offer a distinct characterization of ignition stages. Further HIF experimental tests were given in [13] where various tree branches were tested. The neutral current was given as the most important feature to detect HIFs. Electrical contact between an active conductor and ground was observed to produce changes in the neutral current and a characteristic frequency near the fundamental [13]. Neither [12,13] had any distinct focus on bush species.

This research presents the electrical and physical characterization of phase-to-earth vegetation faults (bush faults from hereafter) for a range of bush species. These include the (i) Banksia Marginata (i.e. Silver Banksia) (ii) Kunzea Ericoides (i.e. Burgan) (iii) Rubus Fruticosus (i.e. Blackberry) (iv) Ulex Europaeus (i.e. Gorse). Vegetation faults have been analyzed in two key categories including "Wire into Bush" (WiB) and "Bush touching Wire" (BtW)

* Corresponding author.
E-mail address: cagil.ozansoy@vu.edu.au (C. Ozansoy).
Peer review under responsibility of Karabuk University.

https://doi.org/10.1016/j.jestch.2020.03.002

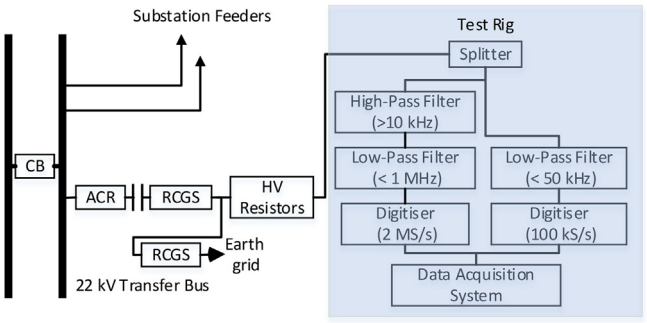

Fig. 1. Test rig and measurement system.

faults. The findings originate from analysis of parameters such as the fault current (I_f), duration to reach a pre-set current threshold, conduction intermittency, and rate of change of the RMS current. Stages of ignition development are discussed as a physical phenomenon and linked to the RMS fault current.

The methodology employs data from a large number of niche staged vegetation High-Impedance Faults (HIFs) performed for the 'Vegetation Conduction Ignition Testing' project [14]. Funded by the Australian government, this project focused on sampling and testing of diverse vegetation species in staged HIFs in a test rig (see Fig. 1). A key outcome was a data set of fault signal recordings used herein for fire ignition analysis. The reader could refer to the Victorian Department website for relevant data and test videos [15].

WiB fault tests included a High Voltage (HV) conductor energized at 12.7 kV dropped into the bush species without touching the ground. For the WiB faults, the bush species was laid horizontally on two parallel conductors, one of which was earthed. The test rig and data acquisition system configuration are illustrated in Fig. 1. One of the two measurement channels was used for the sampling of Low-Frequency (LF) (<50 kHz) current signals. The other channel sampled signals at 2 MS/s with a Nyquist frequency of 1 MHz. In all analyzed tests, the pre-set fault current threshold varied from 0.5 Amps to 4 Amps (through the use of a current limiting resistor). The experiment was terminated by removing the HV supply to the energized conductor once this value was reached.

A study of extreme fire weather days [16] showed that Mildura (a regional center in Victoria) experiences 8.14 days of extreme fire risk days per season on average. Marxsen [14] recommended a 0.5 Amp detection sensitivity setting for extreme fire risk days and argues that "if a power line protection system can detect and

Table 1
Fire-producing bush tests.

Test	Species	Duration to I_{limit} (s)	Type	Moisture (%wt)	D (mm)
0.5 Amp Limit					
VT83	K. E	21.32	BtW	33.6	20
VT84	K. E	N/A	BtW	30.4	–
VT319	K. E	16.71	BtW	32.7	35
VT183	U. E	14.56	WiB	37.7	–
1 Amp Limit					
VT89	K. E	17.5	BtW	36.2	30
VT320	K. E	19.94	BtW	36.3	30
VT504	R. F	7.76	WiB	31.8	15
VT186	U. E	34.32	WiB	40.7	–
VT188	U. E	22.86	WiB	34.3	–
2 Amp Limit					
VT101	K. E	36.34	BtW	41.8	40
VT322	K. E	50.43	BtW	32.3	20
VT505	R. F	3	WiB	43.7	–
VT509	R. F	4.83	WiB	46.9	–
VT515	R. F	4.15	WiB	43.7	–
VT189	U. E	19.68	WiB	37.2	–
VT191	U. E	N/A	WiB	36.1	–
4 Amp Limit					
VT335	B. M	2.68	WiB	61.3	30
VT135	R. F	11.39	WiB	49.3	–
VT138	R. F	6.76	WiB	–	–
VT506	R. F	0.81	WiB	43.7	–
VT133	U. E	N/A	WiB	36	–

Table 2
Ember formation timings in bush tests.

Test	Species	Type	Ember Formation (s)	Duration to I_{limit} (s)
0.5 Amp Limit				
VT83	K. E	BtW	17	21.32
VT84	K. E	BtW	20	N/A
VT319	K. E	BtW	11.9	16.71
1 Amp Limit				
VT89	K. E	BtW	7	17.5
VT320	K. E	BtW	7	19.94
2 Amp Limit				
VT101	K. E	BtW	10	36.34
VT322	K. E	BtW	13	50.43

Please cite this article as: C. Ozansoy and D. P. S. Gomes, Electrical and physical characterization of earth faults for diverse bush species, Engineering Science and Technology, an International Journal, https://doi.org/10.1016/j.jestch.2020.03.002

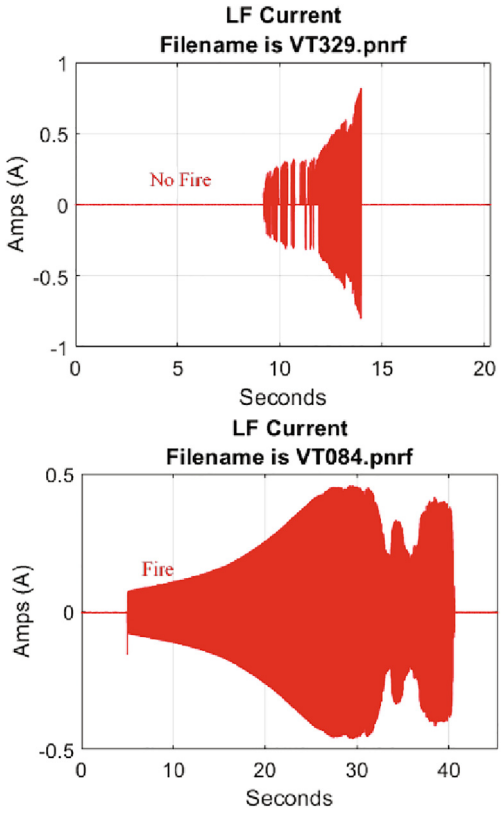

Fig. 2. LF current comparison for fire and no-fore cases.

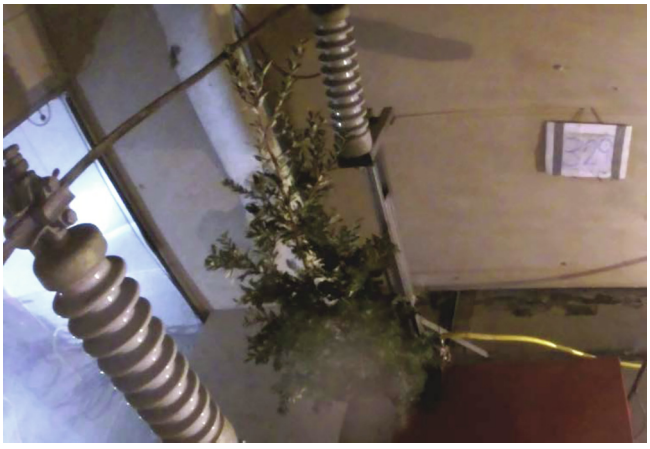

Fig. 3. No-fire result in Test VT329.

respond to an earth-fault drawing 0.5 Amps, fire risk from 'wire into bush' faults might be cut by about 80%" [14]. Previous Rapid Earth Fault Current Limiter (REFCL) Trials [17] at Frankston in 2014 demonstrated reliable fault detection of 1 Amp fault currents with recommendations of 0.5 Amp fault detection sensitivity for extreme fire risk days.

The research problem addressed herein centers on the analysis of the link between phase-to-earth bush faults and vegetative ignition development. The work attempts to discover the link between the HIF current buildup and ignition development on bush species that come in contact with the conductor. The present work aims to answer the following key questions: (i) Do bush faults go through distinct stages of ignition development? (ii) Do all phase-to-earth faults follow the same ignition development regime? (iii) Do these

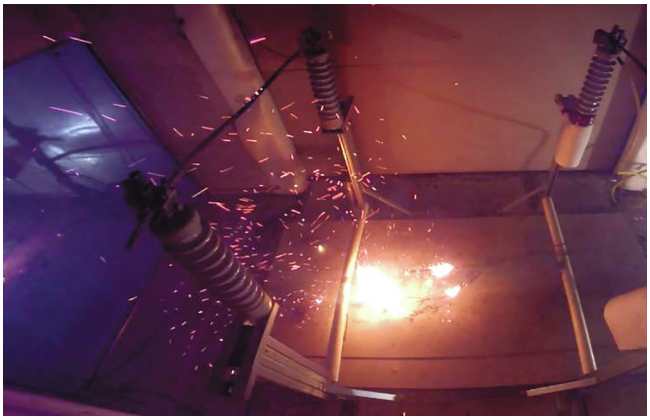

Fig. 4. No-fire result in Test VT329.

stages differ for "Wire into Bush" (WiB) and "Bush touching Wire" (BtW) faults? (iv), and can we analytically observe these ignition stages in the HIF current?

This work makes novel contributions by validating that (i) bush faults with interrupted periods of conduction are less likely to start fires (ii) RMS fault current of a fire producing fault will not have any current conduction intermittency (iii) bush faults go through distinct stages of ignition development that differ between WiB and BtW faults (iv) these distinct stages can be observed from the RMS current and change in the moving average of the RMS current ($\Delta\bar{I}_{f-rms}$) (v) the first zero-crossing in the $\Delta\bar{I}_{f-rms}$occurs before charring begins on a species. In short, the experiments performed here are conceptualized to evidence patterns in the behavior of HIFs resulting in vegetation ignition. This contributes to the understanding of the phenomenon towards contributing to future detection techniques. These goals were achieved through the development of an original methodology capable of pointing to particular characteristics observed during phase-to-earth bush faults.

2. Bush species and phase to earth faults

Table 1 shows the collection of 0.5, 1, 2, and 4 Amp (RMS) pre-set limit fire-producing bush tests. Bush tests resulting in flashover were excluded as flashovers are considered unlikely in real earth faults [14]. For 0.5 Amps limit tests, K. Ericoides was clearly the worst species (with three fire occurrences) leading to the highest probability of fire formation. This is despite K. Ericoides having a moisture content lower than B. Marginata. Table 1 shows the durations for the I_f to reach the respective 0.5–4 Amps (RMS) pre-set values for the fire producing tests; measured when uninterrupted fault current conduction started. This analysis highlights the fire risk based on the speed of I_f. Fault current development speed is critical as it impacts the extent of localized burn (on the species itself) before the power is interrupted. Authors agree with Marxsen [14] that the worst-case scenario is when the fault current takes a long time to reach the preset limit allowing time to ignite and shed glowing embers. For tests VT84-191-133, I_f failed to reach the set threshold. Comparing VT083 and VT319, I_f can be seen to peak to 0.5 Amps faster for the larger diameter VT319 case. This is also true for the comparison between VT101 and VT322.

All fire producing tests have been analyzed in terms of the speed of fire development by watching the videos [15] recorded during the tests. For BtW tests, the duration (after the initial spark at the contact points) for continuous ember formation was observed. In all BtW cases, this occurred well before $\mathbf{I_f}$ reaching

Please cite this article as: C. Ozansoy and D. P. S. Gomes, Electrical and physical characterization of earth faults for diverse bush species, Engineering Science and Technology, an International Journal, https://doi.org/10.1016/j.jestch.2020.03.002

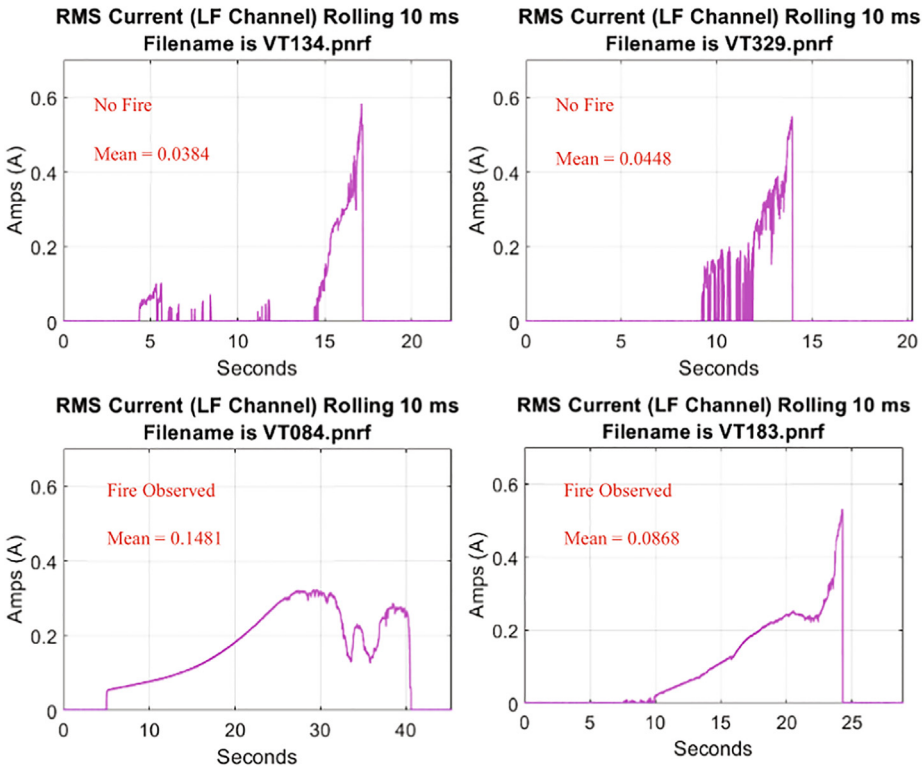

Fig. 5. RMS comparison for fire and no-fire cases (I_{limit} = 0.5 Amps).

the preset limits. Table 2 shows these durations for selected tests. WiB faults, on the other hand, were seen to quickly produce substantial fires within few seconds or almost instantaneously of the conductor being lowered into the species. With some of the WiB faults, the fault drew high currents quickly. Ignition and flame development were as fast for these faults. This raises the question of whether ignition can be avoided in the case of a WiB fault irrespective how quick the protection system can clear the fault.

Analyzing the 0.5-Amp limit tests, ember formation is seen to begin before the pre-set limits were reached. For VT83 and VT319, significant ember formation was observed from the species prior to the pre-set limit. With VT84, the sample burnt so much that it fell on the ground from the two-conductor test rig. In VT183, the sample kept burning even after the conductor was raised away. I_f sensitivity of 0.5 Amp can indeed stop 79% of faults. But, for the 21% 0.5-Amp faults, a different approach is clearly required as one in five fire risk is high. This is especially true in the case of WiB faults, which require a protection system that will perhaps interrupt the current flow whilst the broken conductor is still in the air. For BtW faults, a protection scheme may succeed in significantly reducing the fire risk if it can interrupt current conduction earlier than when $\mathbf{I_f}$ peaks to the pre-set limit.

3. Fire observation

Fig. 2 endorses one key feature of fire causing tests: uninterrupted current conduction. Current recording of VT329 shows intermittent current conduction, interfering with ignition development. Fig. 3 shows a snapshot of the video recording at the end of VT329. As shown, the test did not result in any fire. The current recording of VT084, on the other hand, shows continuous current conduction and fire ignition is evident from the snapshot recorded (see Fig. 4) at the end of this test.

This difference in conduction can be further observed from the rolling RMS current calculation as in Fig. 5. The RMS current has zero (or near zero) values for tests that did not result in fire ignition. In fire-producing tests, the RMS current returns to zero once the test was terminated. The mean RMS value is also significantly higher in fire-producing tests. This leads to the conclusion that RMS current continuity is correlated with faults with higher fire probability. As shown in Fig. 6, odd harmonics are also more evident in fire producing faults; another distinct feature of such faults. It is widely known that one main characteristic of a HIF is the high harmonic current content [18,19]. Up to 15 odd harmonics could be seen in Power Spectral Density analysis for bush HIFs that led to fires. Conversely, less number of odd harmonics are clearly visible in faults that did not result in fire ignition.

4. Analytical analysis to observe stages of ignition progression

Various stages of ignition development can be identified for bush faults [14]. These are the development of contact (Stage 1), expulsion of moisture (Stage 2), and progressive charring (Stage 3). Stage 1 is dominated by a progressive increase in the plasma until I_f reaches its first maximum [14]. In Stage 2, fault current falls due to the expulsion of the moisture which dries out the species leading to its resistance to increase [14]. Finally in Stage 3, charring begins accompanied by break-out of flames. During charring, arcs appear in the flame causing a volatile $\mathbf{I_f}$ [14]. In [14], Marxsen linked these to 'branch on wire' vegetation faults, while the authors have also observed similar patterns for many bush faults discussed herein.

A critical novel contribution herein is that authors have been able to categorize bush faults in three categories: (i) Stage 1 or Stage 3 only faults (ii) three-stage faults and (iii) Stage 1 to Stage 3 faults. Table 3 shows the categorization of twenty one bush faults in terms of stages of ignition development for a range of species.

Please cite this article as: C. Ozansoy and D. P. S. Gomes, Electrical and physical characterization of earth faults for diverse bush species, Engineering Science and Technology, an International Journal, https://doi.org/10.1016/j.jestch.2020.03.002

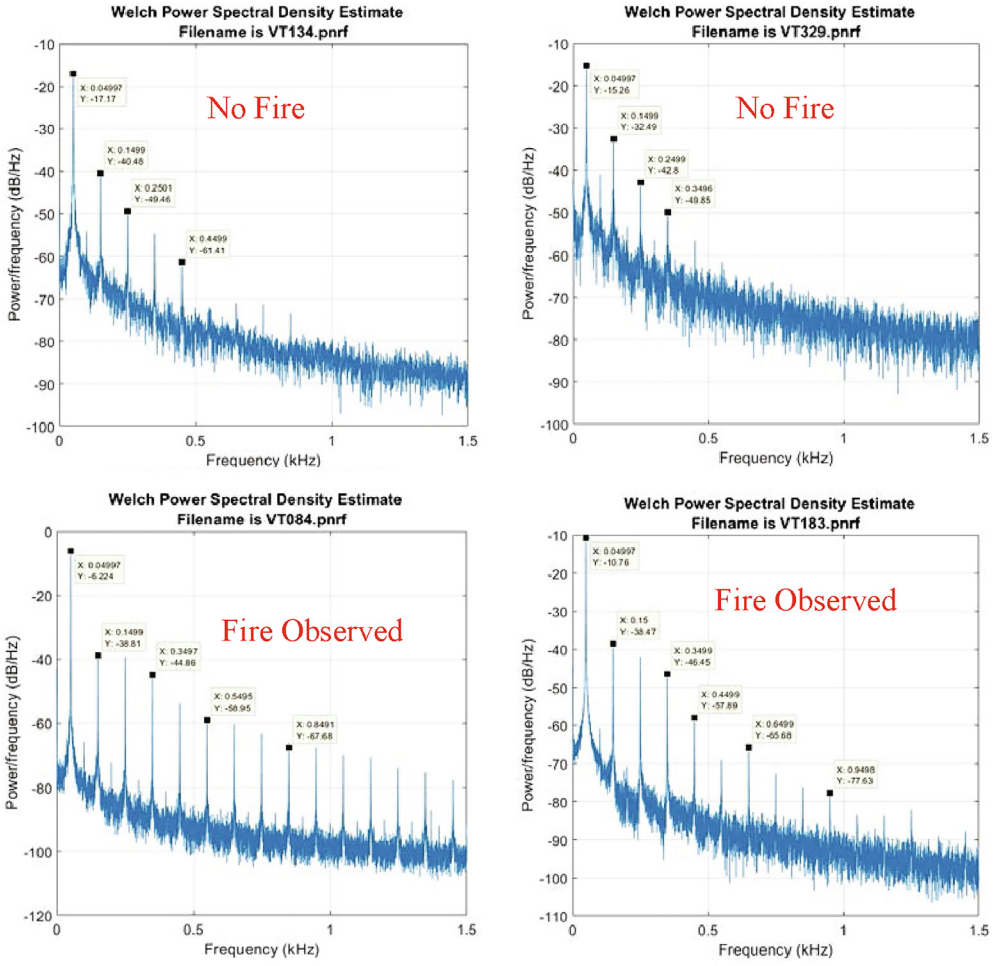

Fig. 6. Odd harmonics for fire and no-fire cases (Ilimit = 0.5 Amps).

Table 3
Ignition development stage analysis.

Test	Pattern	Test	Pattern
VT183	Stages 1, 2, 3	VT135	Stage 1 → Stage 3
VT504	Stage 1	VT138	Stages 1, 2, 3
VT186	Stages 1, 2, 3	VT506	Stage 3
VT188	Stages 1, 2, 3	VT133	Stage 1 → Stage 3
VT505	Stage 3	VT83	Stage 1
VT509	Stage 3	VT84	Stages 1, 2, 3
VT515	Stage 3	VT319	Stage 1
VT189	Stage 1 → Stage 3	VT89	Stage 1
VT191	Stage 1 → Stage 3	VT320	Stage 1
VT335	Stage 3	VT101	Stages 1, 2, 3
		VT322	Stages 1, 2, 3

Fig. 7 shows how these physical properties of a fire can be linked to the fault RMS current and gradient (RMS current rate of change) to substantiate claims. Fig. 7 shows ignition progression for tests VT320-101-515 in three categories (a) Stage 1 only (b) Stages 1, 2, 3 (c) Stage 3 only. Figs. 8 to 10 shows the video recording snapshot of the test species at the conclusion of each test for VT320-101-515.

This paper presents the development of a methodology and associated signal processing to locate these stages of ignition development as a novel contribution. As in Fig. 7, this includes analysis of the rolling RMS current and rate of change of the RMS current. In Fig. 7(a), a Stage 1 only fault is shown for VT320 where sparks are seen at the contact points. During the test, flames extend to the leaves around the vicinity of the contact points but fail to spread over the branch. It is likely that a Stage 1 fault occurred as the test was interrupted once $\mathbf{I_f}$ reached the set threshold very fast. The fire would have perhaps progressed into Stages 2 and 3 had the fault not been interrupted. As shown from the video snapshot (at the conclusion of the test) in Fig. 8, the fire on the species did not extend beyond the leaves above the branch and branch charring is not observed.

Fig. 7(b) shows a low-speed fault current development where the species experienced all three stages of fire ignition. In Stage 1, sparks are seen at the contact points progressively forming flames. In Stage 2, the expulsion of moisture can be observed/heard accompanied by a whistling noise. In Stage 3, flame extends along the branch resulting in charring. The sudden increase in current volatility (a sign of charring) is apparent in Fig. 7(b) enabling researchers to pinpoint the boundary between Stages 2–3. As shown, volatility begins to peak around the first local minimum (after the first maximum). Hence, the claim herein is that by identifying the first maximum and minimum and the increase in the volatility of the gradient of the RMS current, these three stages can be somewhat distinguished. An all-stages fault is a worst-case scenario as fire finds time to ignite and shed embers due to slow development of the fault current. Fig. 9 shows the snapshot at the conclusion of this test. As shown, evidence of charring could be easily identified on one end of the branch.

Fig. 7(c) shows a Stage 3-only test, where due to the fast development of the fault current, fire quickly progresses into Stage 3,

Please cite this article as: C. Ozansoy and D. P. S. Gomes, Electrical and physical characterization of earth faults for diverse bush species, Engineering Science and Technology, an International Journal, https://doi.org/10.1016/j.jestch.2020.03.002

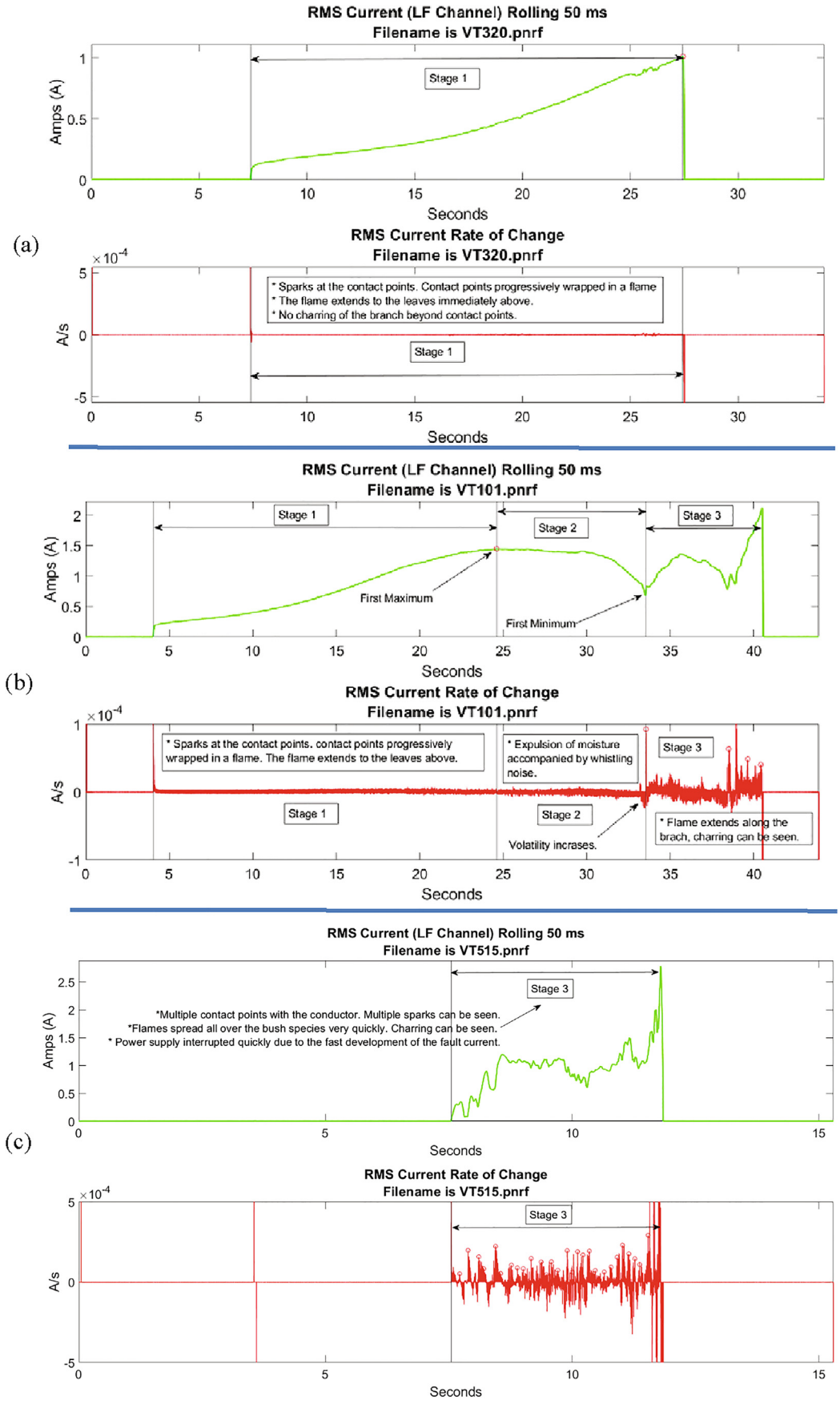

Fig. 7. Progression of fires; (a) Stage 1 only (b) Stages 1, 2, 3 (c) Stage 3 only.

Please cite this article as: C. Ozansoy and D. P. S. Gomes, Electrical and physical characterization of earth faults for diverse bush species, Engineering Science and Technology, an International Journal, https://doi.org/10.1016/j.jestch.2020.03.002

Fig. 8. Video recording snapshot for test VT320.

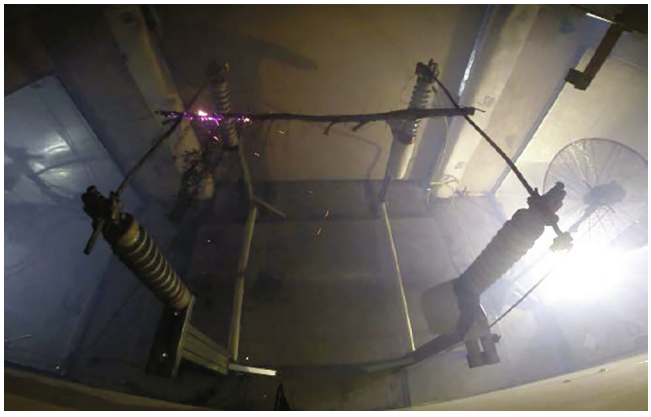

Fig. 9. Video recording snapshot for test VT101.

but is also quickly interrupted by the trip of the power supply. For such fires, relatively low ember formation was observed as the fire is short-lived. Fig. 10 shows the extent of ignition spread on a WiB fault.

It must be noted that with any fire, there are often no clear discrete set-points between phases, i.e. the start and end of each phase are not really precise points. Hence, the claim herein is not that authors can pinpoint each phase precisely, but rather that the proposed methodology allows the identification of borders between these phases. Such estimation works particularly well for transitions between Stages 2 and 3. By watching the staged test videos, the authors confirmed that initiation and spread of flames do begin somewhere on the slope from the first maximum to the first local minimum.

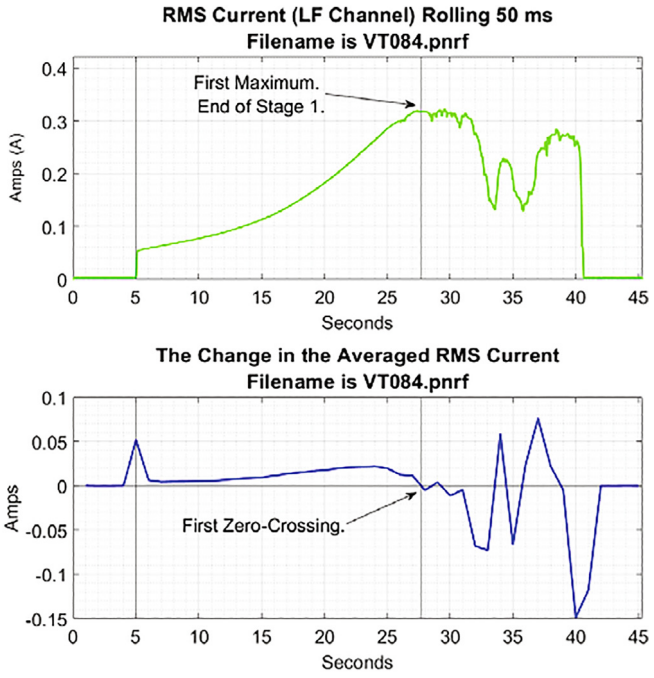

Fig. 11. Algorithm outcome for VT084 (Stages 1 → 2 → 3).

Table 4
First maximum analysis.

Test	Duration to the first maximum (s)	Duration to the current limit (s)	Difference (s)
VT183	11.02	14.56	3.54
VT84	22.68	–	–
VT186	9.45	34.32	24.87
VT188	14.39	22.86	8.47
VT101	21.08	36.34	15.26
VT322	23.40	50.43	27.03
VT189	17.51	19.68	2.17
VT191	11.91	–	–
VT135	5.60	11.39	5.79
VT138	2.24	6.76	4.52
VT133	4.23	–	–

Despite suggesting various stages of ignition during a HIF, the report by Marxsen [14] does not present any significant analytical analysis around these observations. What was presented appeared to be based on visual and audial observations during the tests, as

Fig. 10. Video recording snapshot for test VT515.

Please cite this article as: C. Ozansoy and D. P. S. Gomes, Electrical and physical characterization of earth faults for diverse bush species, Engineering Science and Technology, an International Journal, https://doi.org/10.1016/j.jestch.2020.03.002

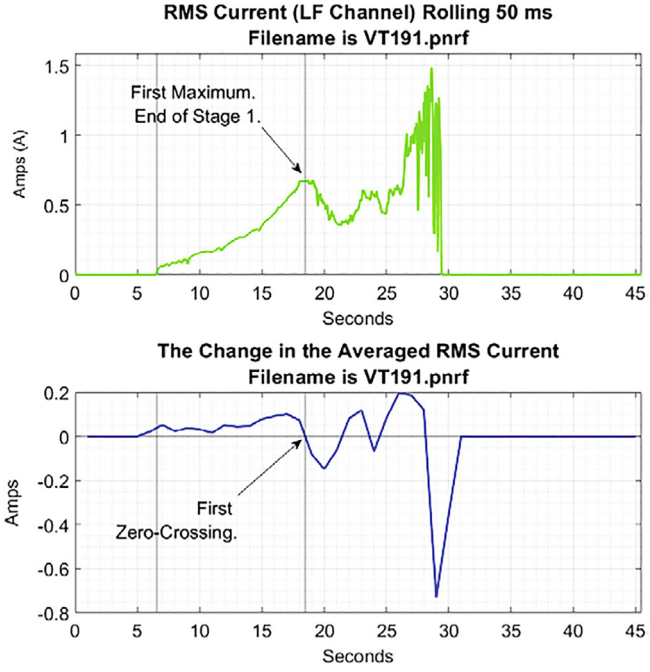

Fig. 12. Algorithm outcome for VT191 (Stages 1 → 3).

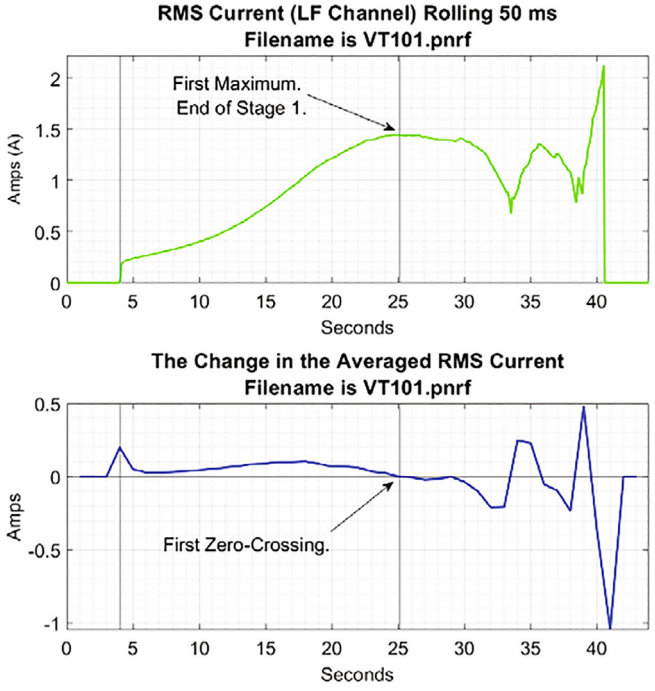

Fig. 13. Algorithm outcome for VT101 (Stages 1 → 2 → 3).

well as on the knowledge of the physical changes in the vegetation samples (such as the increase of resistance due to drying) during periods of conduction. The work herein first demonstrates that a vegetation sample not necessarily goes through all stages of ignition and that the current signals can be processed to yield patterns signifying transition between defined stages of conduction. This particularly includes the analysis of the rolling change in the averaged fault RMS current and rate of change of the RMS current. These attributes set this work aside from [14] and advance the contribution to knowledge in the Marxsen report [14].

One critical aspect of the developed methodology includes the signal processing of the current signal to derive its RMS gradient. It results in clear patterns attesting the increase in the volatility to be a reliable indicator of the fault development from Stage 2 to Stage 3. Section 5 discusses further signal processing of the current signal for calculation of the rolling change in the averaged RMS current, from which zero-crossing can be identified indicative of the different stages. This includes signal processing of the current signal to compute its rolling RMS, its rolling averaging ($I_{f-\overline{rms}}$), and computation of the difference in $I_{f-\overline{rms}}$ for indexed samples. This difference $\Delta I_{f-\overline{rms}}$gives away the zero crossings.

5. Directional Δ in the averaged rolling RMS current

A HIF must ideally be detected before Stage 2 commences, i.e. after the first peak in $I_{f\text{-}rms}$. This could enable interruption of a fire before the spark at the contact points grows into flames igniting any surrounding leaves and before it grows into progressive charring. A method has been devised to identify the Stage 1 crossing which includes calculation of the rolling change in the averaged RMS current ($\Delta\overline{I_{f-rms}}$). First, the 50 ms rolling RMS current is computed in discrete time using Eq. (1), which is then averaged every 100,000 samples (1 s) using Eq. (2). Eq. (3) then allows computing the difference between $\Delta I_{f-\overline{rms}}$ for every (n + 1)th and nth indexed samples.

By detecting the first zero crossing on the $\Delta I_{f-\overline{rms}}$, the approximate boundary between Stage 1 and Stage 2 can be reliably estimated as shown in Figs. 11-13 for tests VT84, VT191, and VT101. These tests were chosen as they never reached the pre-set thresholds. For example, the zero crossing in the $\Delta I_{f-\overline{rms}}$ for test VT084 occurs around the 27.5th second which also corresponds to the first maximum on the rolling RMS current and hence the end of Stage 1.

This approach can't be applied to Stage 3-only or Stage 1-only faults. Yet, the approach is suitable for the worst-case "all stages" and "Stage 1 → 3" faults as shown in Table 4. For all "all stages" and "Stage 1 → 3" faults, the proposed approach was successfully applied to identify the first zero crossings indicative of the end of Stage 1. Table 4 shows a summary of the durations to the first maximum and current limit set points. As shown, the time difference between the two set points ranges from as low as 2.17 s to as high as 27.03 s. In the case of VT322 for example, the species experiences moisture expulsion and charring for a further 27.03 s post the end of Stage 1 which significantly increases the amount of embers falling on the forest bed. If a protection system can respond to a HIF within 5 s of conductor contact with the species, 81% of these fire producing faults can be stopped before progressive charring.

$$I_{f-rms}(i) = \sqrt{\frac{1}{N} \times \sum_{k=i-N+1}^{i} I_f^2(k)} \quad for \;\; i \geq 5000 \tag{1}$$

$$where \;\; N = window \;\; length \times Sampling\_Rate$$

$$where \;\; N = 50ms \times 100,000 \frac{kS}{s} = 5,000$$

$$I_{f-av}(j) = \frac{1}{N} \times \sum_{k=j-N+1}^{j} I_{f-rms}(k) \;\; for \;\; i \geq 100,000 \tag{2}$$

$$where \;\; N = 100,000$$

$$\Delta I_{f-\overline{rms}} = \Delta I_{f-av}(j) = I_{f-av}(j+1) - I_{f-av}(j) \tag{3}$$

Please cite this article as: C. Ozansoy and D. P. S. Gomes, Electrical and physical characterization of earth faults for diverse bush species, Engineering Science and Technology, an International Journal, https://doi.org/10.1016/j.jestch.2020.03.002

6. Conclusion

This paper has presented a method for analyzing the current conduction phenomena in electric faults involving bush species. The work has demonstrated that phase-to-earth bush faults are more likely to cause fire ignition in cases of uninterrupted current conduction. The current signal was analysed and signal processed to derive metrics of relevance, such as the rolling RMS current, its gradient, and rolling average to analytically demonstrate patterns that signify various stages of ignition and increased volatility during a HIF. The rolling RMS current and its gradient were used to identify stages of ignition development including the initial contact and sparks (Stage 1), expulsion of moisture (Stage 2), and extension of flames and charring (Stage 3).

The analysis enabled authors to categorize bush faults in four categories of ignition development. These include (i) Stage 1 only or (ii) Stage 3 only, (iii) all-stages and (iv) Stage 1 to Stage 3 faults. All-stage faults were observed to be the worst-case faults due to the low speed of fault current development causing the fire to progress through all stages of ignition development.

A novel approach has been proposed herein to estimate these stages of ignition development from analysis of the rolling RMS current and change in the averaged RMS current. This is critical as it led to further development of a 'directional change in the averaged rolling RMS current' approach to identify maximum fault clearance times for an effective reduction in the fire risk. The developed hypotheses were tested and validated in all eleven "all-stages" and "Stage 1 to 3" faults with 100% accuracy. Results show that if a protection system can respond to an earth fault within 5 s of conductor contact with the vegetation species, then 81% of these fire igniting faults can be stopped before they grow into progressive charring, which limits the amount of embers falling on a forest bed in a real-life setting.

Declaration of Competing Interest

The authors declare that they have no known competing financial interests or personal relationships that could have appeared to influence the work reported in this paper.

References

[1] S. Kavaskar, N.K. Mohanty, Detection of high impedance fault in distribution networks, Ain Shams Eng. J. 10 (2019) 5–13, https://doi.org/10.1016/j.asej.2018.04.006.

[2] N.I. Elkalashy, M. Lehtonen, H.A. Darwish, M.A. Izzularab, A.I. Taalab, Modeling and experimental verification of high impedance arcing fault in medium voltage networks, IEEE Trans. Dielectr. Electr. Insul. 14 (2007) 375–383, https://doi.org/10.1109/TDEI.2007.344617.

[3] V. Torres, J.L. Guardado, H.F. Ruiz, S. Maximov, Modeling and detection of high impedance faults, Int. J. Electr. Power Energy Syst. 61 (2014) 163–172, https://doi.org/10.1016/j.ijepes.2014.03.046.

[4] N. Bahador, F. Namdari, H.R. Matinfar, Tree-related high impedance fault location using phase shift measurement of high frequency magnetic field, Intern J Electr Pow & En Sys 100 (2018) 531–539, https://doi.org/10.1016/j.ijepes.2018.03.008.

[5] E. Khakimzyanov, R. Mustafin, P. Platonov, Method of fault location for double line-to-earth faults in distribution networks, Eng. Sci. Technol. Int. J. 19 (2016) 1668–1671, https://doi.org/10.1016/j.jestch.2016.09.004.

[6] A.S. Ahmed, M.A. Attia, N.M. Hamed, A.Y. Abdelaziz, Modern optimization algorithms for fault location estimation in power systems, Eng. Sci. Technol. Int. J. 20 (2017) 1475–1485, https://doi.org/10.1016/j.jestch.2017.11.006.

[7] A. Farughian, L. Kumpulainen, K. Kauhaniemi, Review of methodologies for earth fault indication and location in compensated and unearthed MV distribution networks, Electr. Pow. Syst. Res. 154 (2018) 373–380, https://doi.org/10.1016/j.epsr.2017.09.006.

[8] D.P.S. Gomes, C. Ozansoy, A. Ulhaq, J.C. Júnior, The effectiveness of different sampling rates in vegetation high-impedance fault classification, Electr. Pow. Syst. Res. 174 (2019), https://doi.org/10.1016/j.epsr.2019.105872 105872.

[9] A. Ghaderi, H.L. Ginn, H.A. Mohammadpour, High impedance fault detection: a review, Electr. Power Syst. Res. 143 (2017) 376–388, https://doi.org/10.1016/j.epsr.2016.10.021.

[10] K. Sarwagya, S. De, P.K. Nayak, High-impedance fault detection in electrical power distribution systems using moving sum approach, IET Sci. Meas. Technol. 12 (2018) 1–8, https://doi.org/10.1049/iet-smt.2017.0231.

[11] B.K. Chaitanya, A. Yadav, M. Pazoki, An intelligent detection of high-impedance faults for distribution lines integrated with distributed generators, IEEE Syst. J. (2019) 1–10, https://doi.org/10.1109/JSYST.2019.2911529.

[12] J.A. Wischkaemper, C.L. Benner, B.D. Russell, Electrical characterization of vegetation contacts with distribution conductors – investigation of progressive fault behavior, in: 2008 IEEE/PES Transmission and Distribution Conference and Exposition, 2008, pp. 21–24.

[13] P. González, E. Romero, V.M. Miñambres, M.A. Guerrero. Experimental tests of High Impedance Faults in MV rural distribution network, 2014 International Conference on Optimization of Electrical and Electronic Equipment (OPTIM), 2014 22-24 May 2014.

[14] T. Marxsen, Vegetation Conduction Ignition Test Report – Final, Marxsen Consulting Pty Ltd, Department of Economic Development Jobs Transport and Resources, 2015.

[15] Victorian Government. Powerline Bushfire Safety Program – Vegetation Conduction Ignition Test Report and Data. Available from: https://discover.data.vic.gov.au/dataset/powerline-bushfire-safety-program-vegetation-conduction-ignition-test-report. [Accessed on 22 July 2019].

[16] M. Long, A climatology of extreme fire weather days in Victoria, Aust. Meteorol. Mag. 55 (2006) 3–18.

[17] T. Marxsen, REFCL Trial Ignition Tests, Marxsen Consulting Pty Ltd, 2014.

[18] S.M. Shahrtash, M. Sarlak, High Impedance Fault Detection Using Harmonics Energy Decision Tree Algorithm, 2006 International Conference on Power System Technology; 2006 22-26 Oct. 2006.

[19] V. Torres, H.F. Ruiz, S. Maximov, S. Ramírez, Modeling of high impedance faults in electric distribution systems, 2014 IEEE International Autumn Meeting on Power, Electronics and Computing (ROPEC); 2014 5–7 Nov. 2014.

Cagil Ozansoy received his B.Eng. degree in electrical and electronic engineering (Hons.) and his Ph.D. research degree from Victoria University, Melbourne, Australia, in 2002 and 2006, respectively. He is now working as a Senior Lecturer and Researcher in the College of Engineering and Science, Victoria University. His major teaching and research focus is in power systems protection specifically on high impedance fault detection.

Douglas P. S. Gomes received the B.E. degree in electrical engineering from Federal University of Mato Grosso, Brazil, in 2013 and the M.Sc. degree in Power Systems from University of Sao Paulo, Brazil, in 2016. He is currently working towards his Ph.D. degree at Victoria University, Melbourne, Australia. His research interests are power systems, protection, power quality, and artificial intelligent systems.

Please cite this article as: C. Ozansoy and D. P. S. Gomes, Electrical and physical characterization of earth faults for diverse bush species, Engineering Science and Technology, an International Journal, https://doi.org/10.1016/j.jestch.2020.03.002